Analysis of concrete fracture using a novel cohesive crack method

Y. Dong *, S. Wu, S.S. Xu, Y. Zhang, S. Fang

Beijing University of Technology, Department of Engineering Mechanics, China

A R T I C L E   I N F O

A B S T R A C T

Numerical analysis of fracture in concrete is studied with a simplified discrete crack method. The discrete crack method is a meshless method in which the crack is modeled by discrete cohesive crack segments passing through the nodes. The cohesive crack segments govern the non-linear response of concrete in tension softening and introduce anisotropy in the material model. The advantage of the presented discrete crack method over other discrete crack method is its simplicity and applicability to many cracks. In contrast to most other discrete crack methods, no representation of the crack surface is needed. On the other hand, the accuracy of discrete crack methods is maintained. This is demonstrated through several examples.

1. Introduction

The fracture process of structures made of quasi-brittle materials such as concrete is characterized by the formation of microcracks that eventually coalesce and lead to the formation of continuous macrocracks. Though methods exists that smear treat cracking in a smeared sense [1–15], it is believed that many applications require the description of discrete cracks. Crack propagation in concrete materials is associated with localization of the strain field, which, in case of fully open macrocracks becomes singular across the crack. Obviously, numerical analyses of this class of problems require robust models which adequately represent the discontinuous character of the fracture process. For the modeling of the non-linear material behavior in the vicinity of the crack tip cohesive crack models [16–25], which take into account a gradual transition from full material strength to zero material strength, are generally adopted. This is necessary for materials with strain softening since the use of pure continuum models lead to mesh dependent results [26].

Since the mid of the 1960s considerable progress has been made in developing models to describe the evolution of cohesive cracks in quasi-brittle materials using continuum-based approaches such as plasticity or damage formulations, rotating or fixed crack models, which, since the mid of the 1980s, have been enhanced by means of adequate regularization techniques (see, e.g. [1,27–29] for a smeared representations of cracks). At the same time, models allowing for a discrete representation of cracks have been developed by introducing cracks as separate entities directly into the discretization. Meshless methods have become popular for these applications since thanks to the absence of a mesh, discrete cracks can easily be inserted into the discretization [2,30–40]. Though these methods can handle arbitrary crack propagation, they are usually restricted to a few number of cracks due to computational efficiency. One major difficulty of discrete crack models is representation and cracking of crack surface that becomes cumbersome when number of cracks increase. However, concrete

---

* Corresponding author.
  E-mail address: ydong@windowslive.com (Y. Dong).

structures generally undergo excessive cracking before failure. Therefore, numerical methods are needed that can handle many cracks. We propose a method based on an idea developed in [41] that can handle many cracks and simultaneously maintain the accurate character of discrete crack models. That method was successfully used for a variety of problems [42–47]. Such methods are urgently needed to model and understand cracking phenomena in concrete materials.

We present a meshless method for cohesive cracks. The meshless method is based on local partition of unity in order to model the crack. In contrast to most other methods, the crack is described by a set of discrete crack segments through a node. Cohesive zone models are applied at the interfaces of these crack segments in order to take into account the energy dissipation during cracking. The main advantage of the method is its simplicity. There is no need for tracking the crack path. This makes the method well suited for simulation of many cracks as they occur in concrete materials.

2. The methodology – a flow chart

This paragraph briefly outlines the basic steps of the method. One of the key ingredients of the method is the element-free Galerkin method, Section 3, that is capable of modeling arbitrary crack growth. The crack is modeled via local partition of unity enrichment. Therefore, discrete cohesive crack segments are introduced into the element-free Galerkin method through a simple enrichment scheme, Section 4, once a certain cracking criterion is met that is explained in Section 5. The cohesive crack segments are required to pass through the entire domain of influence of a node and the orientation is determined by the cracking criterion, Section 5.

The cohesive force term, Section 6, is introduced as external force into the governing equations, Section 7, and takes into account the energy dissipation during the fracture process avoiding spurious mesh-dependence. The cohesive traction depends on the jump in the displacement field that is given through the partition of unity enriched meshfree method. A flow chart is given in Fig. 1.

3. Element free Galerkin method

The element-free Galerkin (EFG) method [48] is derived from moving-least-squares (MLS) approximation, that can be written in terms of a polynomial basis $\mathbf{p}(\mathbf{x})$ and unknown coefficients $\mathbf{a}(\mathbf{x})$:
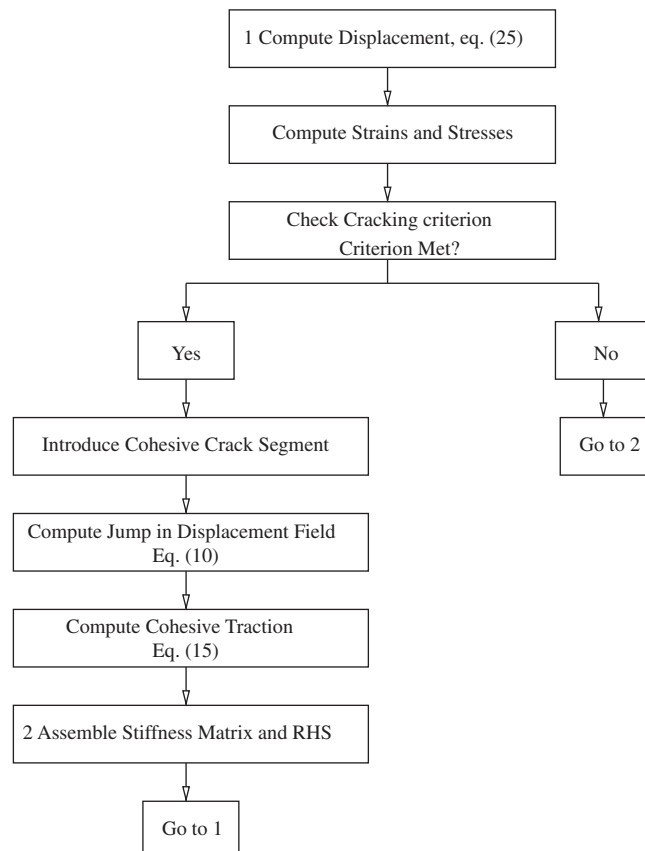

Fig. 1. Flow chart of the proposed method.

$$\mathbf{u}^{con}(\mathbf{x}) = \sum_{I=1}^{NP} p_I(\mathbf{x})a_I(\mathbf{x}). \tag{1}$$

Here, the superimposed *con* denotes the *continuous* character of the approximation, $\mathbf{p}$ is set to $\mathbf{p}^T(\mathbf{x}) = (1,x,y)$ and hence $NP = 3$.

Let us define the discrete weighted $\mathcal{L}_2$ error norm J

$$J = \sum_{I=1}^{N}(\mathbf{P}^T(\mathbf{x}_I)\mathbf{a}(\mathbf{x}_I) - \mathbf{u}_I)^2 w(\mathbf{x} - \mathbf{x}_I, h) \tag{2}$$

with kernel function $w(\mathbf{x} - \mathbf{x}_I, h)$ where h is the interpolation radius of the kernel function, $\mathbf{P}^T(\mathbf{x}_I)\mathbf{a}(\mathbf{x}_I)$ is the matrix expression of Eq. (1) and N is the number of nodes that are within this interpolation radius. The number of nodes N has to be larger (or at least equal) than the number of polynomial functions NP in order to uniquely determine the unknown coefficients $\mathbf{a}$. We chose the quartic B-spline with circular support size for our kernel function:

$$w(\mathbf{x} - \mathbf{x}_I, h) = w(s) = \begin{cases} 1 - 6s^2 + 8s^2 - 3s^4, & s \leqslant 1, \\ 0, & s > 1 \end{cases} \tag{3}$$

with $s = \frac{\mathbf{x}_I - \mathbf{x}_i}{2h}$ for circular support size. The size $2h$ is the interpolation radius and is two times the distance between nodes.

Minimizing J, Eq. (2), with respect to the unknown coefficients $\mathbf{a}$ leads to the final EFG approximation

$$\mathbf{u}^{con}(\mathbf{x}) = \sum_{I=1}^{N} N_I(\mathbf{x})\mathbf{u}_I \tag{4}$$

with the meshless shape functions

$$N_I(\mathbf{x}) = \mathbf{p}^T(\mathbf{x})A^{-1}(\mathbf{x})\mathbf{D}_I(\mathbf{x}) \tag{5}$$

and

$$\mathbf{D}_I(\mathbf{x}) = w(\mathbf{x} - \mathbf{x}_I, h)\mathbf{p}^T(\mathbf{x}_I),$$
$$\mathbf{A}_I(\mathbf{x}) = \sum_I w(\mathbf{x} - \mathbf{x}_I, h)\mathbf{p}(\mathbf{x}_I)\mathbf{p}^T(\mathbf{x}_I). \tag{6}$$

4. Displacement field approximation

Crack is a discontinuity in the displacement field. Therefore, Eq. (4) is complemented with another term that is capable to capture the jump in the displacement field. We can think of decomposing the displacement field into a continuous part $\mathbf{u}^{con}$, Eq. (4), and discontinuous part $\mathbf{u}^{dis}$ that will be defined subsequently:

$$\mathbf{u}(\mathbf{x}) = \mathbf{u}^{con}(\mathbf{x}) + \mathbf{u}^{dis}(\mathbf{x}). \tag{7}$$

To discretize the discontinuous displacement field, we take advantage of the local partition of unity [49] method, local means that the approximation is only modified in the vicinity of the crack. The partition of unity concept is especially useful in the context of material failure since the kinematics of the crack can be incorporated into the formulation elegantly.

Instead of describing the crack as continuous surface, we propose to model the discrete crack by discrete cohesive crack segments that pass through the entire domain of influence of a node, Fig. 2. This circumvents the need of tracking the crack path. The jump in the displacement field is obtained by the discontinuous displacement approximation that is active only for nodes that contain the cohesive crack segments:

$$\mathbf{u}^{dis}(\mathbf{x}) = \sum_{I \in \mathcal{W}_c} N_I(\mathbf{x})\Psi(\mathbf{x})\mathbf{q}_I, \tag{8}$$

where $\mathcal{W}_c$ is the set of enriched nodes, $\mathbf{q}_I$ are additional unknowns and $\Psi(\mathbf{x})$ is the enrichment function:

$$\Psi(\mathbf{x}) = \begin{cases} 1 & \text{if } \mathbf{n} \cdot (\mathbf{x} - \mathbf{x}_I) > 0, \\ -1 & \text{if } \mathbf{n} \cdot (\mathbf{x} - \mathbf{x}_I) > 0. \end{cases} \tag{9}$$

Note that only cracked nodes are enriched. The length of the cohesive segment is equal to the size of the domain of influence of the associated cracked node. The jump in the displacement field $[[\mathbf{u}]] = \mathbf{u}^{\Omega_+} - \mathbf{u}^{\Omega}$, where the subscript of Ω indicates the different sides of the crack, Fig. 3, only depends on the additional degrees of freedom $\mathbf{q}_I$:

$$[[\mathbf{u}(\mathbf{x})]] = \sum_{I \in \mathcal{W}_c} 2N_I(\mathbf{x})\mathbf{q}_I. \tag{10}$$

Instead of using the step function, Eq. (9), the heaviside enrichment could for instance be used that would result in pure positive enriched shape functions. The factor of 2 would then disappear in Eq. (10). In fact, any discontinuous function can be
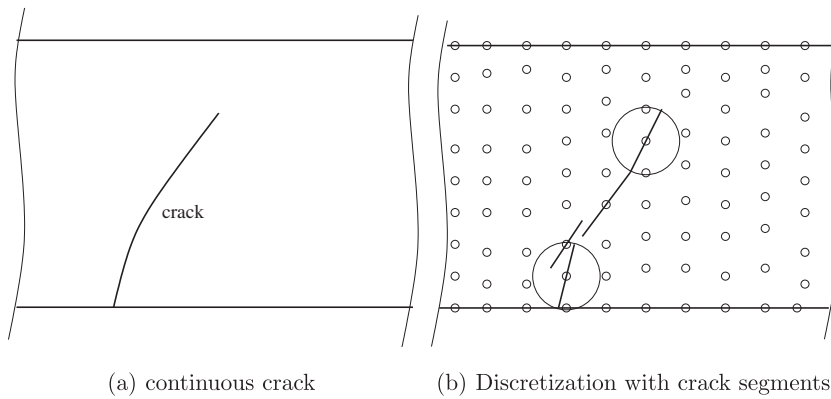
(a) continuous crack   (b) Discretization with crack segments

Fig. 2. (a) Continuous crack and (b) representation of the crack with discrete cohesive crack segments.
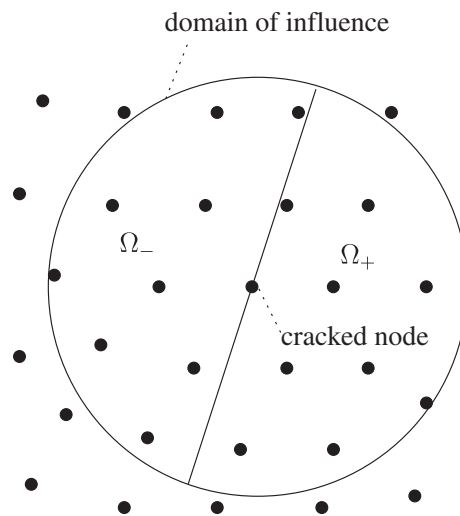

Fig. 3. Cracked node where the crack segment crosses the entire domain of influence of the node.

used in order to model the jump in the displacement field. The additional nodal degrees of freedom q would adjust automatically. We choose the step function since it result in a symmetric enriched shape function.

The discrete strain field can be derived as

$$\nabla \mathbf{u}^s(\mathbf{x}) = \sum_{I \in \mathcal{W}} \nabla N_I(\mathbf{x}) \mathbf{u}_I + \sum_{I \in \mathcal{W}_c} \nabla N_I(\mathbf{x}) \Psi(\mathbf{x}) \mathbf{q}_I, \tag{11}$$

where $\mathcal{W}$ is the set of all nodes and $\mathcal{W}_c$ is the set of cracked nodes.

5. Cracking criterion

We used the Rankine criterion to generate a crack. The crack is introduced once the maximum principal tensile stress exceeds the uni-axial tensile strength. The orientation of the crack is defined by the vector n and parallel to the direction of the maximum principal tensile stress. The principal stresses (and their orientation) are obtained via the solution of the eigenvalue problem:

$$(\sigma_{ij} - \sigma_p \delta_{ij}) n_j = 0. \tag{12}$$

σ_p being the eigenvalue, i.e. the principal stress, and n_j being the associated eigenvector that determines the orientation of the principal stress and hence the orientation of the crack.

To avoid erratic crack patterns, the stress field in the vicinity of cracked nodes are averaged. The non-local stress tensor $\bar{\bar{\mathbf{P}}}$ is computed as a weighted average of the stresses at NG Gauss points. It results from the sum of the local stresses $\mathbf{P}_I$ at the Gauss points I, weighted with $\hat{w}_I$ and the associated area A_I:
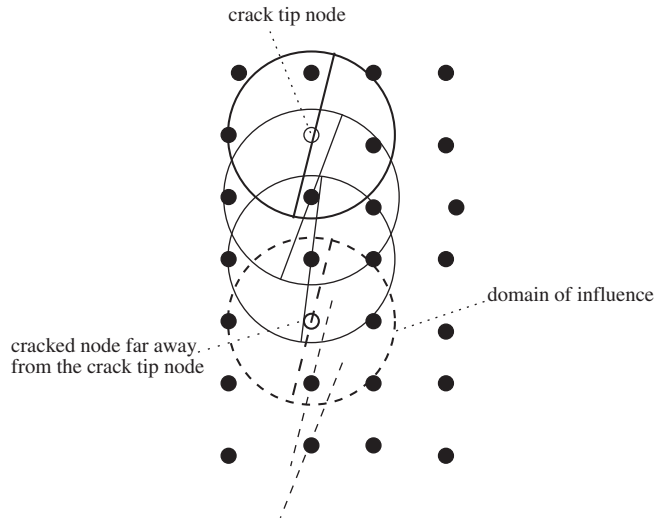
Fig. 4. Fixed crack segments illustrated by dashed lines for nodes far away from the crack segment of the node at the tip. Rotated crack segments are illustrated by solid lines.

$$\overline{\mathbf{P}} = \sum_I^{NG} \mathbf{P}_I \hat{w}_I A_I \tag{13}$$

with

$$\hat{w}(s) = \frac{w(s)}{\sum_I^{NG} w_I A_I}, \tag{14}$$

where $w(s)$ is the quartic B-spline.

The stress field will change when the crack propagates. The Rankine criterion for crack initiation is met when only small changes of the principal (stress) axes occur. Therefore, we allow the crack segments to rotate according to changes of the direction of principal stress axis. This avoids artificial cracking of already existing macro-cracks far away from the crack tip (see Fig. 4).

6. The cohesive law

In general, cohesive traction appear normal to the crack and in tangential direction as e.g. pointed out by [18,50]. In this manuscript, we neglect cohesive tractions in tangential direction and leave the influence of the cohesive traction in tangential direction. This is indeed a simplification but other authors that deal with similar problems with more complex numerical methods [31,49,51–58] reported good results. Since we also aim a direct comparison to those methods and our focus is on the numerical method, we aim to remove other influences as much as possible.

In the cohesive model, the traction is related to the crack opening, Eq. (10):

$$t_n = f_t - \frac{f_t}{\delta_{max}} [[u]]_n \quad \text{if } [[u]]_n < \delta_{max} \quad \text{and} \quad [[u]]_n^{t+\Delta t} > [[u]]_n^t$$

$$\text{otherwise } t_n = 0 \text{ when } [[u]]_n^{t+\Delta t} > [[u]]_n^t, \tag{15}$$

where

$$[[u]]_n = \mathbf{n} \cdot [[\mathbf{u}]] \tag{16}$$

is the crack opening and δ_{max} is the point where the traction have decayed to zero. Unloading is linear elastic. We neglected shear traction in our studies but intend to incorporate them in the future.

7. Equilibrium equations and discretization

The equation of equilibrium is given by

$$\nabla \cdot \mathbf{P} + \mathbf{b} = \mathbf{0}, \quad \mathbf{x} \in \Omega, \tag{17}$$

$$\mathbf{u} = \bar{\mathbf{u}}, \quad \mathbf{x} \in \Gamma_u, \tag{18}$$

$$\mathbf{n}_t \cdot \mathbf{P} = \bar{\mathbf{t}}, \quad \mathbf{x} \in \Gamma_t, \tag{19}$$

$$\mathbf{n}_c \cdot \mathbf{P} = \mathbf{t}_c([[\mathbf{u}]]), \quad \mathbf{x} \in \Gamma_c, \tag{20}$$

where **u** are the displacements, **t** are the tractions, **P** is the stress tensor, **b** are the body forces, Γ is the boundary and the subscript u, t, c denote "displacement", "traction" and "crack", respectively. With the test functions **v** that are of similar structure than the trial functions, Eqs. (4), (8), the weak form of the equations of equilibrium can be assembled:

$$\sum_{j=1}^{n} \left[\int_{\Omega_j} \nabla^s \mathbf{v}_j : \mathbf{P} \, d\Omega + \int_{\Gamma_{cj}} \mathbf{v} \cdot \mathbf{t}_c \, d\Gamma \right] = \sum_{j=1}^{n} \int_{\Gamma_{tj}} \mathbf{v} \cdot \bar{\mathbf{t}} \, d\Gamma. \tag{21}$$

Inserting the trial functions, Eqs. (8) and (4), and the test functions that are of similar structure into Eq. (21), the equation to be solved is given in matrix form:

$$\int_{\Omega} \widehat{\mathbf{B}}^T \mathbf{P} \, d\Omega + \int_{\Gamma_c} \widehat{\mathbf{N}}^T \mathbf{t}_c \, d\Gamma = \int_{\Gamma_t} \widehat{\mathbf{N}}^T \bar{\mathbf{t}} \, d\Gamma + \int_{\Omega} \widehat{\mathbf{N}}^T \mathbf{b} \, d\Omega, \tag{22}$$

where $\widehat{\mathbf{B}}$ and $\widehat{\mathbf{N}}$ contain continuous and discontinuous shape functions and their spatial derivatives, respectively. Continuous B-matrix:

$$\mathbf{B}_I^u = \begin{bmatrix} N_{I,x} & 0 \\ 0 & N_{I,y} \\ N_{I,y} & N_{I,x} \end{bmatrix}. \tag{23}$$

Discontinuous B-matrix:

$$\mathbf{B}_I^q = \begin{bmatrix} \widetilde{N}_{I,x} & 0 \\ 0 & \widetilde{N}_{I,y} \\ \widetilde{N}_{I,y} & \widetilde{N}_{I,x} \end{bmatrix} \tag{24}$$

with $\widetilde{N} = N \Psi(\mathbf{x})$.

The final system of equations

$$\begin{bmatrix} \mathbf{K}_{IJ}^{uu} & \mathbf{K}_{IJ}^{uq} \\ \mathbf{K}_{IJ}^{qu} & \mathbf{K}_{IJ}^{qq} \end{bmatrix} \cdot \begin{bmatrix} \Delta \mathbf{u}_J \\ \Delta \mathbf{q}_J \end{bmatrix} = \begin{bmatrix} \mathbf{f}_{I,ext}^{u} - \mathbf{f}_{I,int}^{u} \\ \mathbf{f}_{I,ext}^{q} - \mathbf{f}_{I,int}^{q} \end{bmatrix} \tag{25}$$

is solved with an incremental iteration scheme in which

$$\mathbf{K}_{IJ}^{ij} = \int_{\Omega} (\mathbf{B}_I^i)^T \mathbf{C} \, \mathbf{B}_J^j \, d\Omega + \kappa \int_{\Gamma_c} \mathbf{N}^T \mathbf{D} \mathbf{N} \, d\Gamma, \tag{26}$$

where $\kappa = 1$ when $i = j = q$, otherwise $\kappa = 0$, **D** is the tangential stiffness of the cohesive model and the superscript i and j indicate u and q for the continuous and discontinuous shape functions and

$$\mathbf{f}_{I,ext}^{i} = \int_{\Gamma_t} \left(\mathbf{N}_I^i \right)^T \mathbf{t} \, d\Gamma + \int_{\Omega} \left(\mathbf{N}_I^i \right)^T \mathbf{b} \, d\Omega, \tag{27}$$

$$\mathbf{f}_{I,int}^{i} = \int_{\Omega} \left(\mathbf{B}_I^i \right)^T \mathbf{P} \, d\Omega + \int_{\Omega} \left(\mathbf{N}_I^q \right)^T \mathbf{t}_c \, d\Gamma. \tag{28}$$

The integrals are evaluated by Gauss quadrature. Therefore, a background mesh is constructed such that the EFG nodes span the background mesh. More detailed about Gauss quadrature in the EFG method can be found e.g. in [59,60].

8. Results

After validation of our method, we present three examples: The first example is a pre-notched sample under four-point bending. The second example is mixed-mode failure of concrete and the last example is a three-point bending beam that develops several cracks.

8.1. Validation

To validate our method, we studied examples where an analytical solution is available. We present results for plate under uni-axial tension, Fig. 5. We solved this problem with three different methods:

- Finite element method with bilinear quadrilateral shape functions.
- EFG method with visibility criterion.
- Crack segment method.

In the finite element analysis, the crack is aligned with the crack. In the crack segment method, the crack segments are placed in the middle of the specimen. The error in the energy norm is shown in Fig. 6a. The meshless methods are more accu-
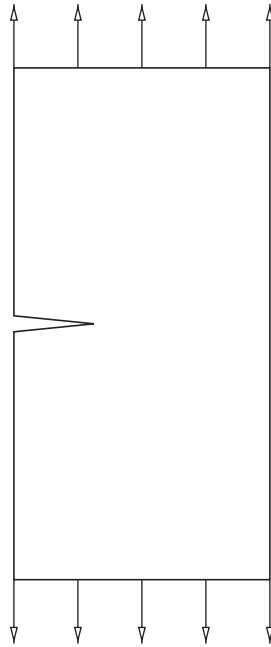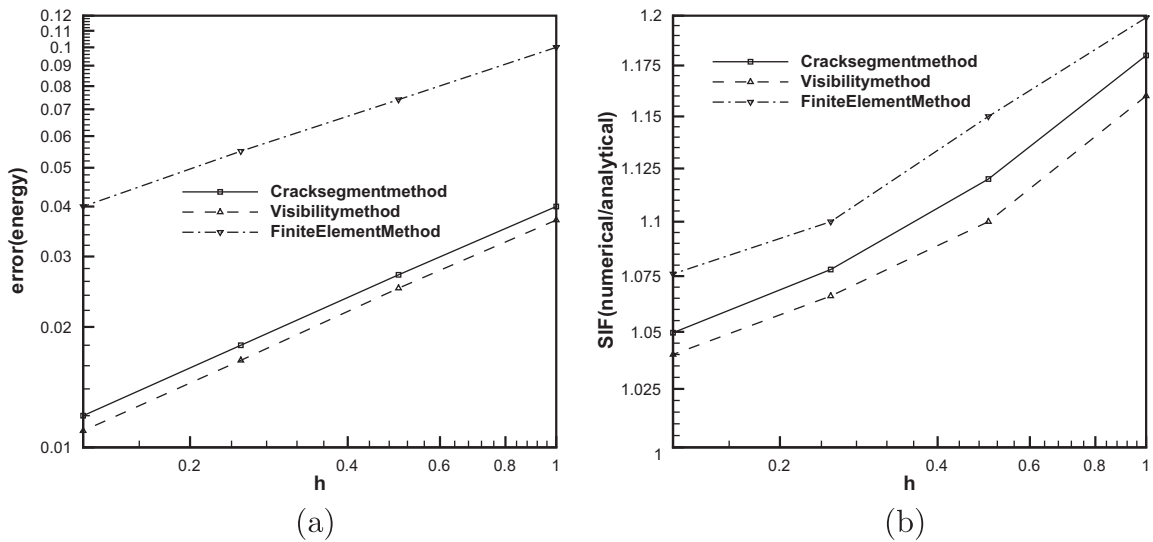
Fig. 5. Plate in tension.

Fig. 6. Results for the plate in tension.

rate than the finite element method. The crack segment method is of the same accuracy as the EFG method with visibility criterion but the crack segment method is computationally more efficient since it does not require representation of crack surface. Fig. 6b shows the stress intensity factor (SIF) K_I for the problem. Visibility method and crack segment method are more accurate than finite element method and the crack segment method is similar to visibility method.

8.2. Tensile-shear beam

Consider the pre-notched beam in Fig. 7 that is subjected to concentrated forces F. Experimental data was reported by [61]. The beam has a rectangular cross-section with thickness 156 mm. The pre-notch has a length of 82 mm. The material's Young's modulus is $E = 25,000$ MPa, Poisson's ratio $v = 0.2$, tensile strength $f_t = 2.8$ MPa and fracture energy $G_f = 100$ N/m.

The crack propagates from the pre-notch obliquely. Initially shear stresses dominate the crack orientation. In the later stage, dominant tensile stresses cause the crack to straighten. Fig. 8 shows the crack pattern at the end of the simulation.
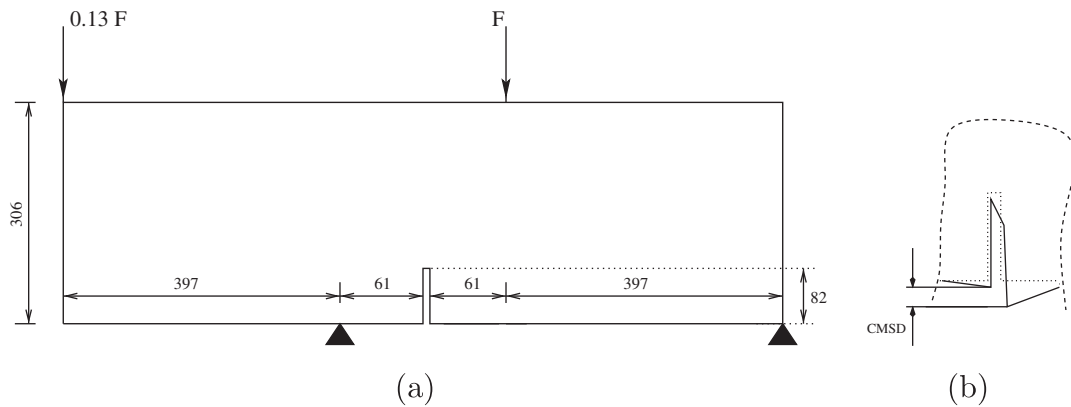
Fig. 7. (a) The pre-notched beam subject to two concentrated loads; all dimensions are in mm and (b) definition CMSD (Crack Mouth Sliding Displacement).

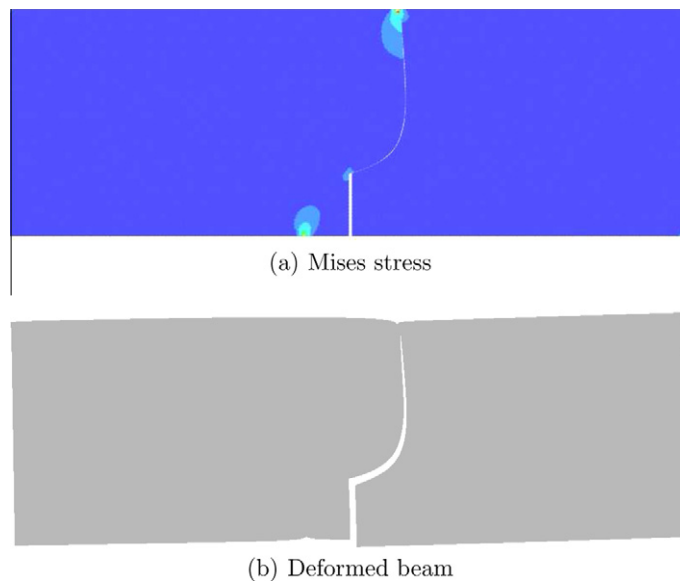(a) Mises stress

(b) Deformed beam

Fig. 8. Crack in the tensile-shear beam.

The load–Crack Mouth Sliding Displacement (CMSD) curve is in close agreement with the load–deflection curve reported in [61]. The definition of CMSD is shown in Fig. 7. The ultimate load in the numerical simulation for the coarsest discretization is 0.134 MN and the ultimate load for the finest discretization is 0.137 MN, that agrees well with the experiments from [61] (see Fig. 9).

8.3. Nooru-Mohamed test

Next example is the mixed-mode fracture test of [62]. A double notched specimen as depicted in Fig. 10 is loaded simultaneously in tension and shear. In the experiment, the shear force is first increased up to a certain value while the tensile force is kept zero. Then, the shear force is kept constant while the tensile force is increased until the specimen fails. We consider displacement control experiments with

(1) shear force = 5 kN;
(2) shear force = 27.38 kN.

In the first case, the crack paths was almost straight while a curved crack paths occurs for case two. This experiment is often used to test numerical methods.

The material parameters for this problem are Young's modulus $E = 36.0$ GPa, Poisson's ratio $v = 0.22$, tensile strength $f_t = 2.2$ MPa and fracture energy $G_f = 100.0$ N/m.
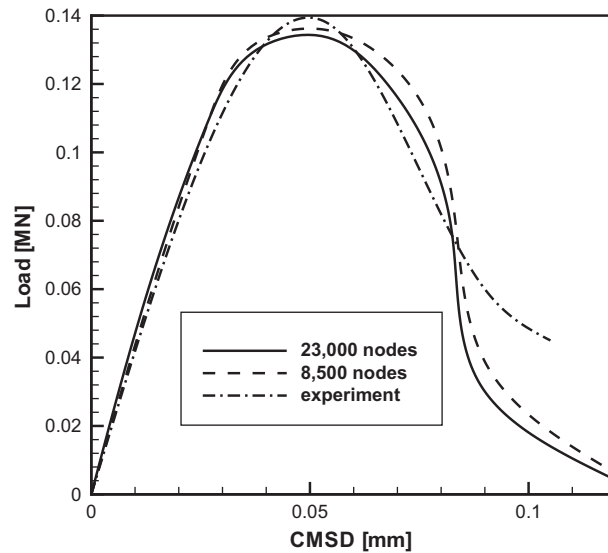
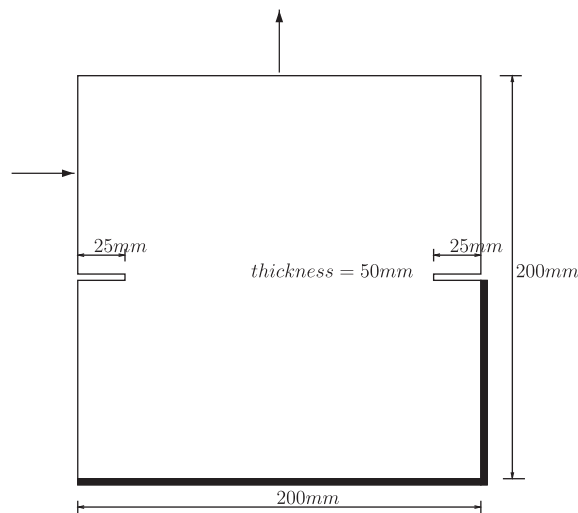**Fig. 9.** Load vs. Crack Mouth Sliding Displacement.

Fig. 10. Nooru-Mohamed mixed-mode test [62].

The crack paths and stress distribution for our numerical simulation is illustrated in Fig. 11. We capture the straight as well as the curved crack paths as they approximately occurred in the experiment. Fig. 12 compares the load displacement curves of simulation and experiment. The ultimate load for simulation 1 is 14.5 kN that deviates around 10% from the experimental ultimate load. The ultimate load for simulation 2 is −2.03 kN and the deviation to the experiment is within 15%. Note the experiments underly a certain deviation as well.

8.3.1. Three-point bending beam

The last example is the three-point bending beam in bending illustrated in Fig. 13. There are five little vertical imperfections (pre-cracks) of 2 mm length in order to facilitate crack propagation.

The material has a Young's modulus $E = 36,000$ MPa, Poisson's ratio $v = 0.2$, tensile strength $f_t = 3$ MPa, $\delta_{max} = 0.33$ mm and fracture energy $G_f = 100$ N/m. Initially, bending stresses are dominant at crack initiation at the bottom and cracks propagate perpendicular to the bottom line. The cracks incline due to shear stresses at a later stage. Fig. 14 shows the crack pattern at the end of the simulation. There is no experimental data available but the crack pattern looks reasonable. The ultimate load is 15.5 kN.
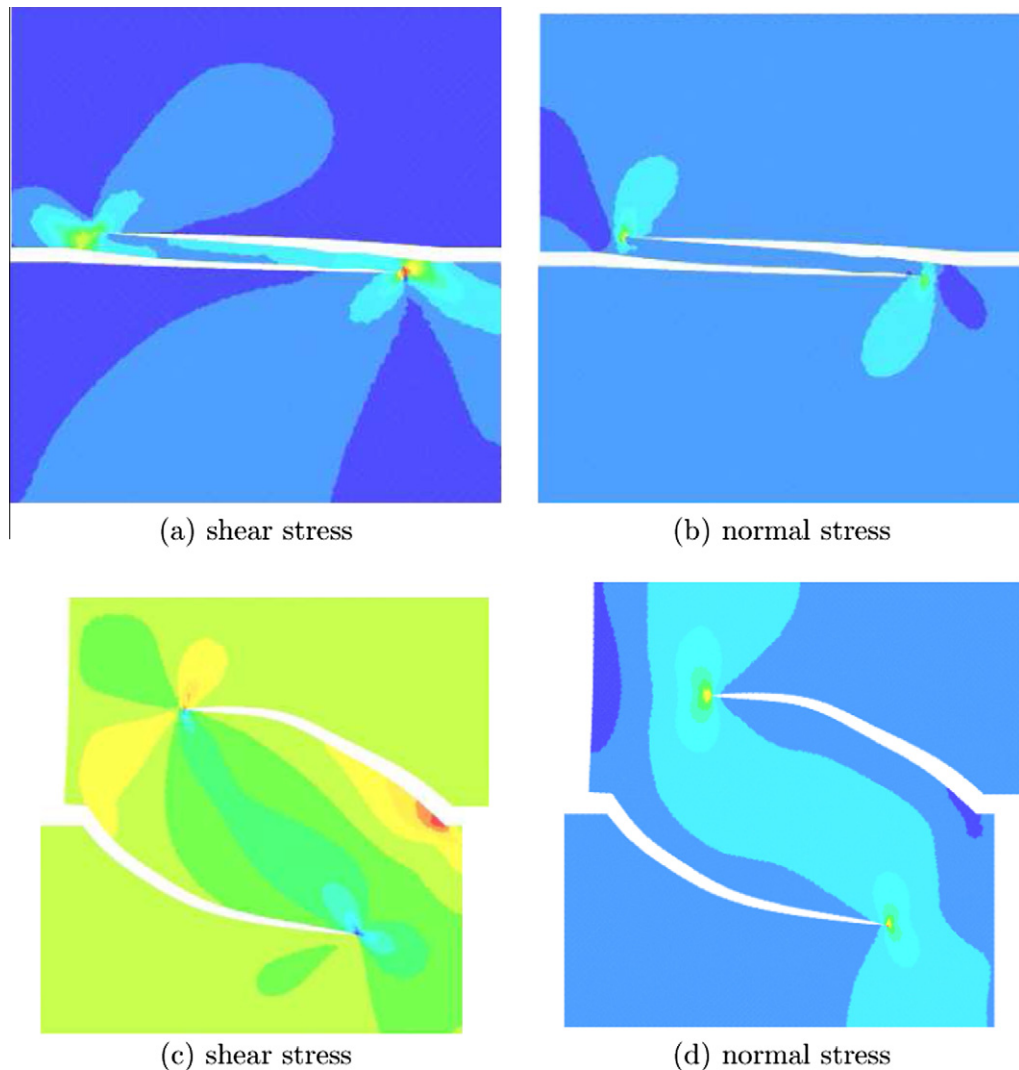
Fig. 11. Results for the Nooru-Mohamed test: (a,b) for a shear force of 5kN and (c,d) for a shear force of 27.38 kN.

8.4. Four-point shear test

The last example to demonstrate the applicability of our method is the four-point shear test experimentally studied by [63]. This test is particularly challenging for numerical methods and was studied with complex discrete crack methods. The experimental set-up is shown in Fig. 15. The ratio of the applied forces F_1/F_2 was set equal to the geometry parameters c/S and the ratio c/D is set to 0.4. The thickness of all specimen was 100 mm. To test size effects, [63] varied the size of the specimen:

(1) Model 1: D = 50 mm;
(2) Model 2: D = 100 mm;
(3) Model 3: D = 200 mm.

The ultimate load increased therefore with increasing height (and length) D. The ultimate load for Model 1 was 19.6 kN, the ultimate load of Model 2 was 32.3 kN and the ultimate load of Model 3 was 58.8 kN that perfectly matches the experimental observations. We use plane stress assumption and the following material parameters [63]: Young's modulus E = 36.53 GPa, Poisson's ratio v = 0.22, tensile strength f_t = 2.18 MPa and fracture energy G_f = 93.0 N/m.

The fracture patterns of the three model are illustrated in Fig. 16. A strong size effect occurs that is also observed experimentally. Two cracks appear for the small specimen while for Model 3 only one main crack reaches the opposite side of the specimen.
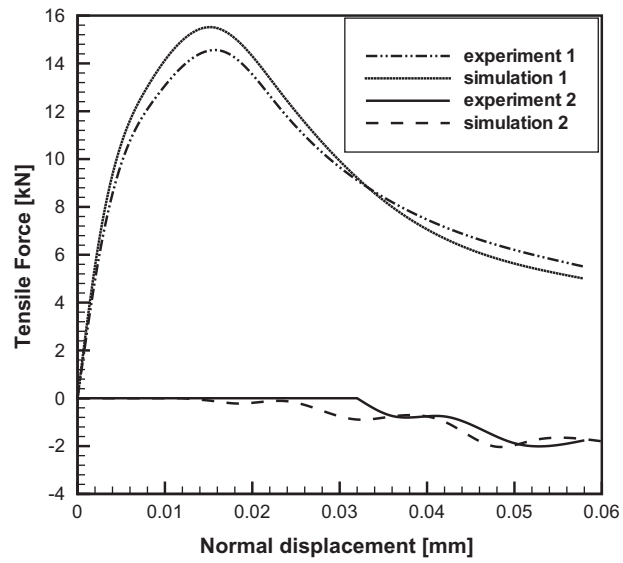
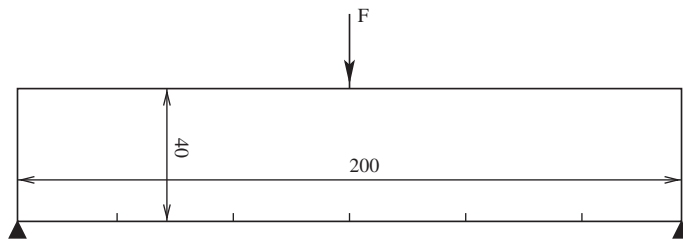**Fig. 12.** Tensile force–normal displacement curve for the Nooru-Mohamed tests.

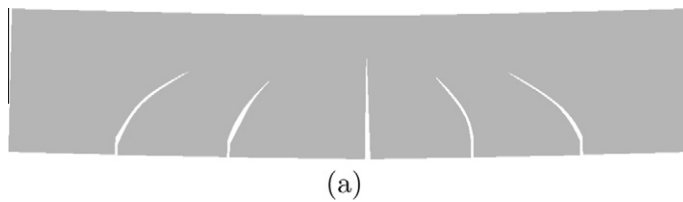**Fig. 13.** Three-point beam in bending, all dimensions are in mm.

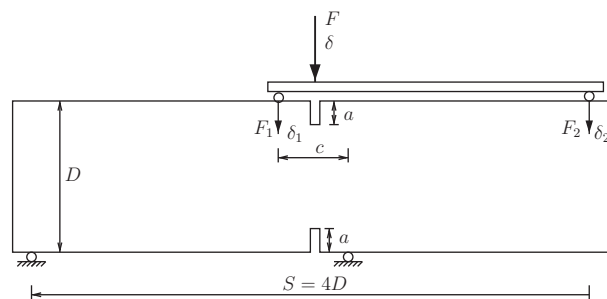**Fig. 14.** Cracks in the three-point bending beam.

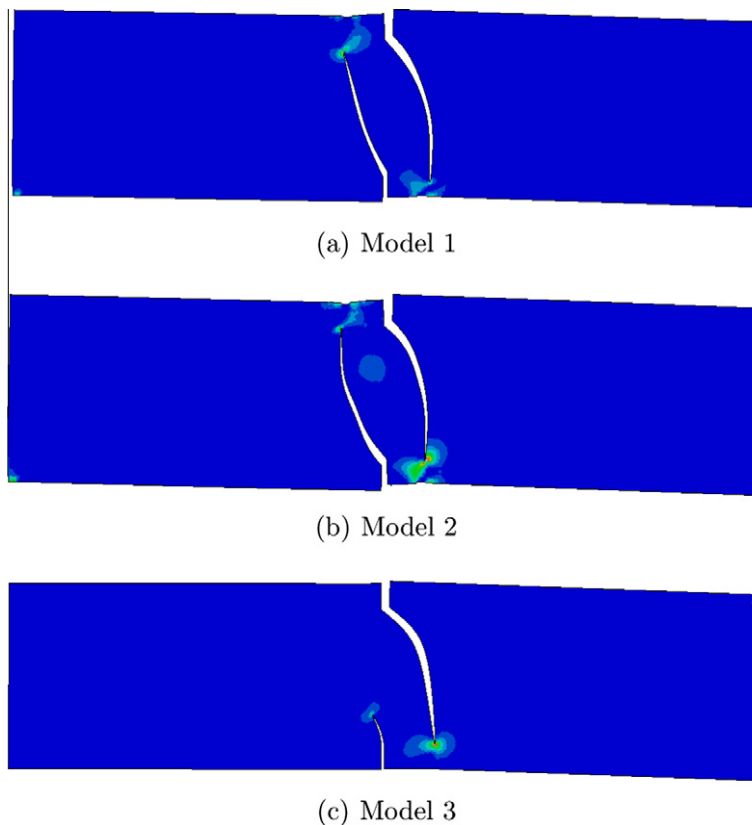**Fig. 15.** Four-point shear test: test set-up.

Fig. 16. Fracture pattern and contour plot of maximum tensile stress of four-point shear test for different specimen sizes.

9. Conclusions

We studied fracture of concrete structure with a simplified meshless method. Therefore, fracture is modeled with discrete crack model. Modeling of fracture is important for assessment and reliability analysis of concrete structures. Since the global response is influenced by local phenomena such as cracking, a detailed crack model is needed. In our discrete crack method, the crack was modeled by a set of cohesive crack segments that directly pass through the nodes such that no representation of the crack surface is necessary. This makes the method ideally suited for concrete due to occurrence of many cracks in the concrete material. It simultaneously maintains the high accuracy of discrete crack methods.

In the future, we will extend the method to reinforced and fibre reinforced concrete structures with bigger dimensions. These structures undergo excessive cracking. They are currently developed at our Institute and our method will be extended to predict the behavior of these structures.

References

[1] Z.P. Bazant, B.H. Oh, Crack band theory for fracture in concrete, Mater. Struct. 16 (1983) 155–177.
[2] S. Hao, W.K. Liu, P.A. Klein, A.J. Rosakis, Modeling and simulation of intersonic crack growth, Int. J. Solids Struct. 41 (7) (2004) 1773–1799.
[3] E. Papa, A. Nappi, Numerical modelling of masonry: a material model accounting for damage effects and plastic strains, Appl. Math. Model. 21 (6) (1997) 319–335.
[4] A. Ray, S. Tangirala, S. Phoha, Stochastic modeling of fatigue crack propagation, Appl. Math. Model. 22 (3) (1998) 197–204.
[5] M. Jirasek, T. Zimmermann, Analysis of rotating crack model, J. Eng. Mech. 124 (1998) 842–851.
[6] L.J. Malvar, M.E. Fourney, A three dimensional application of the smeared crack approach, Eng. Fract. Mech. 35 (1–3) (1990) 251–260.
[7] J. Dorgan, A mixed finite element implementation of a gradient-enhanced coupled damage-plasticity model, Int. J. Damage Mech. 15 (2006) 201–235.
[8] T. Rabczuk, J. Eibl, Simulation of high velocity concrete fragmentation using SPH/MLSPH, Int. J. Numer. Methods Eng. 56 (2003) 1421–1444.
[9] T. Rabczuk, J. Eibl, L. Stempniewski, Numerical analysis of high speed concrete fragmentation using a meshfree Lagrangian method, Eng. Fract. Mech. 71 (4–6) (2004) 547–556.
[10] T. Rabczuk, J. Eibl, Numerical analysis of prestressed concrete beams using a coupled element free Galerkin/finite element method, Int. J. Solids Struct. 41 (3–4) (2004) 1061–1080.
[11] T. Rabczuk, T. Belytschko, Adaptivity for structured meshfree particle methods in 2d and 3d, Int. J. Numer. Methods Eng. 63 (11) (2005) 1559–1582.
[12] T. Rabczuk, J. Akkermann, J. Eibl, A numerical model for reinforced concrete structures, Int. J. Solids Struct. 42 (5–6) (2005) 1327–1354.
[13] T. Rabczuk, J. Eibl, Modelling dynamic failure of concrete with mesh-free methods, Int. J. Impact Eng. 32 (11) (2006) 1878–1897.
[14] R.K. Abu Al-Rub, G.Z. Voyiadiis, A finite strain plastic damage model for high velocity impact using combined viscosity and gradient localization limiters. Part I: Theoretical formulation, Int. J. Damage Mech. 15 (2006) 293–334.

[15] A.R. Khan, A.H. Al-Gadhib, M.H. Baluch, Elasto-damage model for high strength concrete subjected to multiaxial loading, Int. J. Damage Mech. 16 (2007) 361–398.
[16] G. Barenblatt, The mathematical theory of equilibrium of cracks in brittle fracture, Adv. Appl. Fract. 7 (1962) 55–129.
[17] A. Hillerborg, M. Modeer, P.E. Peterson, Analysis of crack formation and crack growth in concrete by means of fracture mechanics and finite elements, Cement Concrete Res. 6 (1976) 773–782.
[18] M. Ortiz, Y. Leroy, A. Needleman, Finite element method for localized failure analysis, Comput. Methods Appl. Mech. Eng. 61 (1987) 189–213.
[19] X.-P. Xu, A. Needleman, Numerical simulations of fast crack growth in brittle solids, J. Mech. Phys. Solids 42 (1994) 1397–1434.
[20] I. Carol, C.M. Lopez, O. Roa, Micromechanical analysis of quasi-brittle materials using fracture-based interface elements, Int. J. Numer. Methods Eng. 52 (1996) 193–215.
[21] J.C. Galves, J. Cervenka, D.A. Cendon, V. Saouma, A discrete crack approach to normal/shear cracking of concrete, Cement Concrete Res. 32 (10) (2002) 1567–1585.
[22] K.M. Lee, J.H. Park, A numerical model for elastic modulus of concrete considering interfacial transition zone, Cement Concrete Res. 38 (3) (2008) 396–402.
[23] T. Rabczuk, G. Zi, A. Gerstenberger, W.A. Wall, A new crack tip element for the phantom node method with arbitrary cohesive cracks, Int. J. Numer. Methods Eng. 75 (2008) 577–599.
[24] T. Rabczuk, S. Bordas, G. Zi, On three-dimensional modelling of crack growth using partition of unity methods, Comput. Struct., in press, doi:10.1016/j.compstruc.2008.08.010.
[25] T. Rabczuk, G. Zi, S. Bordas, H. Nguyen-Xuan, A geometrically nonlinear three dimensional cohesive crack method for reinforced concrete structures, Eng. Fract. Mech. 75 (2008) 4740–4758.
[26] V.V. Bolotin, Fracture from the standpoint of nonlinear stability, Int. J. Non-linear Mech. 29 (4) (1994) 569–585.
[27] Z.P. Bazant, T. Belytschko, Wave propagation in a strain softening bar: exact solution, J. Eng. Mech. ASCE 11 (1985) 381–389.
[28] X.H. Yang, C.Y. Chen, Y.T. Hu, Damage analysis and fracture criteria for piezoelectric ceramics, Int. J. Non-linear Mech. 40 (9) (2005) 1204–1213.
[29] U. Haussler-Combe, J. Hartig, Formulation and numerical implementation of a constitutive law for concrete with strain-based damage and plasticity, Int. J. Non-linear Mech. 43 (5) (2008) 399–415.
[30] R. De Borst, Modern domain-based discretization methods for damage and fractures, Int. J. Fract. 138 (1–4) (2006) 241–-262.
[31] D. Organ, M. Fleming, T. Terry, T. Belytschko, Continuous meshless approximations for nonconvex bodies by diffraction and transparency, Comput. Mech. 18 (1996) 225–235.
[32] S. Hao, W.K. Liu, C.T. Chang, Computer implementation of damage models by finite element and meshfree methods, Comput. Methods Appl. Mech. Eng. 187 (3–4) (2000) 401–440.
[33] S. Hao, W.K. Liu, D. Qian, Localization-induced band and cohesive model, J. Appl. Mech. – Trans. ASME 67 (4) (2000) 803–812.
[34] T. Rabczuk, P.M.A. Areias, T. Belytschko, A meshfree thin shell method for non-linear dynamic fracture, Int. J. Numer. Methods Eng. 72 (2007) 524–548.
[35] S. Li, Bo C. Simonson, Meshfree simulation of ductile crack propagation, Int. J. Comput. Methods Eng. Sci. Mech. 6 (2003) 1–19.
[36] S. Hao, W.K. Liu, Moving particle finite element method with super-convergence: nodal integration formulation and applications, Comput. Methods Appl. Mech. Eng. 195 (44–47) (2006) 6059–6072.
[37] S. Bordas, T. Rabczuk, G. Zi, Three-dimensional crack initiation, propagation, branching and junction in non-linear materials by extrinsic discontinuous enrichment of meshfree methods without asymptotic enrichment, Eng. Fract. Mech. 75 (2008) 943–960.
[38] T. Rabczuk, S. Bordas, G. Zi, A three-dimensional meshfree method for continuous multiple crack initiation, nucleation and propagation in statics and dynamics, Comput. Mech. 40 (3) (2007) 473–495.
[39] T. Rabczuk, P. Areias, A meshfree thin shell for arbitrary evolving cracks based on an extrinsic basis, Comput. Model. Eng. Sci. 16 (2) (2006) 115–130.
[40] T. Rabczuk, R. Gracie, J.-H. Song, T. Belytschko, Immersed particle method for fluid–structure interaction, Int. J. Numer. Methods Eng. 81 (2010) 48–71.
[41] T. Rabczuk, T. Belytschko, Cracking particles: a simplified meshfree method for arbitrary evolving cracks, Int. J. Numer. Methods Eng. 61 (13) (2004) 2316–2343.
[42] T. Rabczuk, T. Belytschko, Application of particle methods to static fracture of reinforced concrete structures, Int. J. Fract. 137 (1–4) (2006) 19–49.
[43] T. Rabczuk, P.M.A. Areias, A new approach for modelling slip lines in geological materials with cohesive models, Int. J. Numer. Anal. Methods Geomech. 30 (11) (2006) 1159–1172.
[44] T. Rabczuk, T. Belytschko, A three dimensional large deformation meshfree method for arbitrary evolving cracks, Comput. Methods Appl. Mech. Eng. 196 (2007) 2777–2799.
[45] T. Rabczuk, P.M.A. Areias, T. Belytschko, A simplified meshfree method for shear bands with cohesive surfaces, Int. J. Numer. Methods Eng. 69 (5) (2007) 993–1021.
[46] T. Rabczuk, E. Samaniego, Discontinuous modelling of shear bands using adaptive meshfree methods, Comput. Methods Appl. Mech. Eng. 197 (2008) 641–658.
[47] T. Rabczuk, J.-H. Song, T. Belytschko, Simulations of instability in dynamic fracture by the cracking particles method, Eng. Fract. Mech. 76 (2009) 730–741.
[48] T. Belytschko, Y.Y. Lu, L. Gu, Element-free Galerkin methods, Int. J. Numer. Eng. 37 (1994) 229–256.
[49] J.M. Melenk, I. Babuska, The partition of unity finite element method: basic theory and applications, Comput. Methods Appl. Mech. Eng. 139 (1996) 289–314.
[50] A. Needleman, A continuum model for void nucleation by inclusion debonding, J. Appl. Mech. – Trans. ASME 54 (1987) 525–531.
[51] T. Belytschko, Y.Y. Lu, Element-free Galerkin methods for static and dynamic fracture, Int. J. Solids Struct. 32 (1995) 2547–2570.
[52] T. Belytschko, Y.Y. Lu, L. Gu, Crack propagation by element-free Galerkin methods, Eng. Fract. Mech. 51 (2) (1995) 295–-315.
[53] T. Belytschko, Y. Krongauz, D. Organ, M. Fleming, P. Krysl, Mesh-less methods: an overview and recent developments, Comput. Methods Appl. Mech. Eng. 139 (1996) 3–47.
[54] G.N. Wells, Discontinuous Modelling of Strain Localisation and Failure, Ph.D. Thesis, Technische Universiteit Delft, The Netherlands, 2001.
[55] G. Ventura, J. Xu, T. Belytschko, A vector level set method and new discontinuity approximation for crack growth by EFG, Int. J. Numer. Methods Eng. 54 (6) (2002) 923–944.
[56] J. Oliver, A.E. Huespe, P.J. Sanchez, A comparative study on finite elements for capturing strong discontinuities: E-fem vs x-fem, Comput. Methods Appl. Mech. Eng. 195 (2006) 4732–4752.
[57] G. Zi, T. Rabczuk, W. Wall, Extended meshfree methods without branch enrichment for cohesive cracks, Comput. Mech. 40 (2) (2007) 367–382.
[58] T. Rabczuk, G. Zi, A meshfree method based on the local partition of unity for cohesive cracks, Comput. Mech. 39 (6) (2007) 743–760.
[59] J. Dolbow, T. Belytschko, An introduction to programming the mesh-less element free Galerkin method, Arch. Comput. Methods Eng. 5 (3) (1998) 207–241.
[60] T. Rabczuk, T. Belytschko, S.P. Xiao, Stable particle methods based on Lagrangian kernels, Comput. Methods Appl. Mech. Eng. 193 (2004) 1035–1063.
[61] M. Arrea, A.R. Ingraffea, Mixed-mode crack propagation in mortar and concrete, Technical Report 81-13, Department of Structural Engineering, Cornell University, New York, 1982.
[62] M.B. Nooru-Mohamed, Mixed-Mode Fracture of Concrete: An Experimental Approach, Ph.D. Thesis, Delft University of Technology, 1992.
[63] E. Ballatore, A. Carpinteri, G. Ferrara, G. Melchiorri, Mixed mode fracture energy of concrete, Eng. Fract. Mech. 35 (1990) 145–157.